Zintl Clusters Hot Paper

How to cite: *Angew. Chem. Int. Ed.* **2020**, *59*, 17286–17290
International Edition: doi.org/10.1002/anie.202008276
German Edition: doi.org/10.1002/ange.202008276

σ-Aromaticity-Induced Stabilization of Heterometallic Supertetrahedral Clusters $[Zn_6Ge_{16}]^{4-}$ and $[Cd_6Ge_{16}]^{4-}$

Hong-Lei Xu[+], Ivan A. Popov[+], Nikolay V. Tkachenko[+], Zi-Chuan Wang, Alvaro Muñoz-Castro, Alexander I. Boldyrev, and Zhong-Ming Sun**

Abstract: *In this work, the largest heterometallic supertetrahedral clusters, $[Zn_6Ge_{16}]^{4-}$ and $[Cd_6Ge_{16}]^{4-}$, were directly self-assembled through highly-charged $[Ge_4]^{4-}$ units and transition metal cations, in which 3-center–2-electron σ bonding in Ge_2Zn or Ge_2Cd triangles plays a vital role in the stabilization of the whole structure. The cluster structures have an open framework with a large central cavity of diameter 4.6 Å for Zn and 5.0 Å for Cd, respectively. Time-dependent HRESI-MS spectra show that the larger clusters grow from smaller components with a single $[Ge_4]^{4-}$ and $ZnMes_2$ units. Calculations performed at the DFT level indicate a very large HOMO–LUMO energy gap in $[M_6Ge_{16}]^{4-}$ (2.22 eV), suggesting high kinetic stability that may offer opportunities in materials science. These observations offer a new strategy for the assembly of heterometallic clusters with high symmetry.*

Supertetrahedral clusters, which are made out of the small tetrahedral building blocks arranged in a tetrahedral fashion, have an intrinsic appeal due to their high symmetry. They have found applications in a wide range of areas, from photolysis to fast-ion conductivity.[1] The flexibility of choice in sub-units has led to a diverse range of structures, many of which involve transition metals in combination with tetrelide or chalcogenide ions. Perhaps, the most high-profile supertetrahedra are the gold clusters Au_{20} and Au_{40} which have been studied extensively in the gas phase and have shed light on the nature of metal-metal bonding.[2] As yet, however, no analogues have been stabilized in the solid state, and it remains a substantial challenge to synthetic chemistry to achieve this goal. One of the most important design tools available to the synthetic chemist is "self-assembly", which allows simple building blocks to be used to construct complex and highly symmetric nanostructures. In the majority of cases, it remains the case that the architecture of the self-assembled product depends on a judicious choice of organic ligand and careful control of reaction conditions as well as chemical bond manipulation such as hydrogen bonds, van der Waals forces, and aurophilic interactions.[3] It is anticipated that small metal clusters are very good candidates for the assembly of large heterometallic clusters. However, to the best of our knowledge, such kind of self-assemblies is very rare and still remains a challenging task. Herein, we report the successful self-assembly of two unprecedented heterometallic supertetrahedral clusters using highly charged $[Ge_4]^{4-}$ as building blocks and transition metals, Zn or Cd, as connection nodes.

The anionic clusters $[M_6Ge_{16}]^{4-}$ (M = Zn (**1a**); Cd (**2a**)) were obtained from the reaction of $K_{12}Ge_{17}$ with $ZnMes_2$/$CdMes_2$ (Mes = 2, 4, 6-$Me_3C_6H_2$) together with 2,2,2-crypt in solutions of N,N-dimethylformamide (DMF)/ethylenediamine (en), Figure 1 A.

Overall, the 22 atoms of the cluster define a highly symmetric concave polyhedron containing 24 Ge_3 and Ge_2M triangles and 4 chair-like concave M_3Ge_3 hexagons (for example: Zn1-Ge3-Zn3-Ge7-Zn5-Ge11). Rather long Zn-Zn and Cd-Cd distances (3.30–3.39 Å and 3.50–3.66 Å, respectively) suggest that direct interactions between the transition metal ions are not a major stabilizing factor. Alternatively, the clusters can be viewed as containing four discrete $[Ge_4]^{4-}$ units at the vertices of the tetrahedron, with a transition metal ion (Zn^{2+}/Cd^{2+}) bridging each edge. The assembly of four Ge_4 units and the associated bridging metal ions creates a large cavity at the center of the clusters with the dimension of 4.6 Å (**1a**) or 5.0 Å (**2a**) (as measured by the distance from one metal to the opposite Ge). The coordination about each Zn/Cd is rather unusual in that it is approximately planar, with the four bonded Ge atoms in a single plane. There is precedent for such geometries in metal ions with a d^{10} configuration, such as $[\eta^2{:}\eta^2\text{-}(Sb_2Sn_2)Au^I\text{-}(Sb_2Sn_2)]^{3-}$,[4] but approximately tetrahedral coordination is a norm for d^{10} ions, as for example in $[\eta^2{:}\eta^2\text{-}Sn_4Au^ISn_4]^{7-}$ and other analogues.[5] The three Ge-Ge bonds of the coordinated edges of the Ge_4 units (2.709–2.717 Å in **1a**, 2.721–2.752 Å in **2a**) are elongated substantially compared to those in the isolated $[Ge_4]^{4-}$ anion (2.574–2.587 Å),[6] while the three non-coordinated Ge-Ge bonds in each Ge_4 unit are, conversely, slightly shorter than those in $[Ge_4]^{4-}$ and other Zn/Ge clusters.[5d,6b,7] The structure of **1a** can usefully be compared

[*] H.-L. Xu,[+] Dr. Z.-C. Wang, Prof. Dr. Z.-M. Sun
Tianjin Key Lab of Rare Earth Materials and Applications, State Key Laboratory of Elemento-Organic Chemistry, School of Materials Science and Engineering, Nankai University
Tianjin 300350 (China)
E-mail: sunlab@nankai.edu.cn
Dr. I. A. Popov[+]
Theoretical Division, Los Alamos National Laboratory
Los Alamos, NM 87545 (USA)
N. V. Tkachenko,[+] Prof. Dr. A. I. Boldyrev
Department of Chemistry and Biochemistry, Utah State University
0300 Old Main Hill, Logan, UT 84322-0300 (USA)
E-mail: a.i.boldyrev@usu.edu
Prof. Dr. A. Muñoz-Castro
Grupo de Química Inorgánicay Materiales Moleculares, Facultad de Ingenieria, Universidad Autonoma de Chile
El Llano Subercaseaux, Santiago 2801 (Chile)
[+] These authors contributed equally to this work.
Supporting information and the ORCID identification number(s) for the author(s) of this article can be found under https://doi.org/10.1002/anie.202008276.

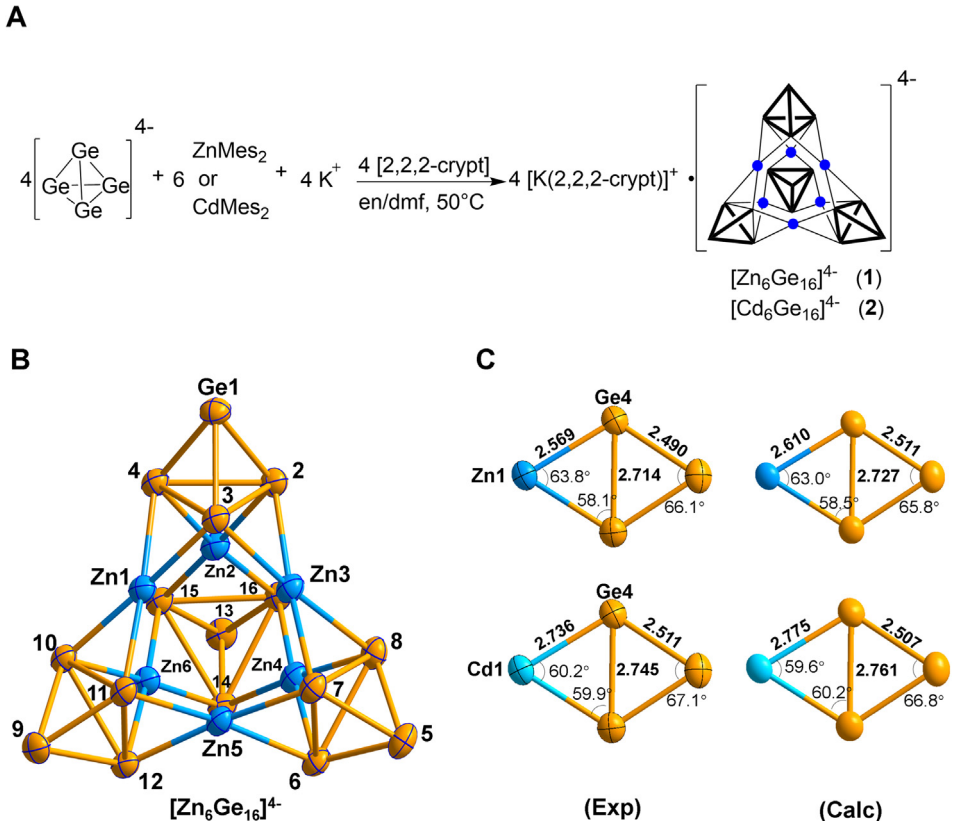

Figure 1. A) Formation scheme of $[M_6Ge_{16}]^{4-}$ (M = Zn or Cd); B) Ellipsoid plot (50% level) of the crystal structure of $[Zn_6Ge_{16}]^{4-}$ (the same structure for $[Cd_6Ge_{16}]^{4-}$); C) The experimental and computed geometries of the Ge-Ge_2-M unit in $[M_6Ge_{16}]^{4-}$ and the average distances of Ge-M and Ge-Ge are given in Å.

to the $[(Ge_4)Zn(Ge_4)]^{6-}$ anion, which is found in two distinct isomeric forms in Cs_6ZnGe_8 and $K_{14}ZnGe_{16}$, where the two Ge_4 units are coordinated η^3:η^3 and η^3:η^2, respectively.[8] The Zn-Ge bond lengths in **1a** lie in a narrow range between 2.547 and 2.589 Å (average 2.569 Å, Figure 1C), slightly shorter than those in both of the above cases. The most direct comparison for **2a** is with $[Cd_3(Ge_3P)_3]^{3-}$ which contains both η^3 and η^2 coordinated Ge_3P units,[9] where the Cd-Ge bond lengths are ≈2.819 Å, similar to those in **2a** (average 2.736 Å).

The assembly of $[Zn_6Ge_{16}]^{4-}$ was followed by time-dependent ESI-MS (Figure S6). After 5 minutes, the reaction mixture is dominated by ions containing a single Ge_4 unit, $\{[K(2,2,2\text{-crypt})][Ge_4Zn_2Mes_2]\}^-$ and $\{[K(2,2,2\text{-crypt})][Ge_4Zn_2Mes_4]\}^-$, at $m/z = 1074.94$ and 1313.11, respectively. After 30 minutes the peaks due to $Ge_4Zn_2Mes_x$ ($x = 2, 4$) have disappeared, and were replaced by four new peaks due to $\{[K(2,2,2\text{-crypt})][Zn_6Ge_{16}]\}^-$, $\{[K(2,2,2\text{-crypt})]_3[Zn_6Ge_{16}]\}^-$ and two intermediate species $\{[K_3(2,2,2\text{-crypt})][ZnGe_8]\}^-$ and $\{[K(2,2,2\text{-crypt})][Zn_3Ge_8Mes_4]\}^-$. The fact that the peak of the $ZnGe_8$ fragment in the ESI-MS is very prominent confirms that it is stable in solution. After 90 minutes, the signals due to $\{[K_3(2,2,2\text{-crypt})][ZnGe_8]\}^-$ and $\{[K(2,2,2\text{-crypt})][Zn_3Ge_8Mes_4]\}^-$ are relatively reduced in intensity relative to the targeted products. At no point do we find evidence for intermediate $Zn_x(Ge_4)_y$ fragments containing more Zn or Ge_4 units, suggesting that the initial Zn-Ge bond formation event is followed by rapid assembly into the final $[Zn_6Ge_{16}]^{4-}$ cluster. Based on the above analysis, a possible assembly mechanism of $[Zn_6Ge_{16}]^{4-}$ is proposed in Figure 2. It is noted that $ZnGe_8$ may be the key intermediate in the formation of **1a**, two $ZnGe_8$ units together with two $ZnMes_2$ species can be directly assembled into ultimate supertetrahedral structure.

To explore the origins of high stability of the $[M_6Ge_{16}]^{4-}$ clusters, we have carried out a series of density functional theory (DFT) calculations using a large polarized quadruple-zeta basis with DFT hybrid functional (PBE0/Def2-QZVP level of theory)[10,11] as implemented in the Gaussian 16 software package[12] (see the Supporting Information for computational details). The highest occupied molecular orbital (HOMO) is triply degenerate (t_1) and is made up of linear combinations of the Ge bonding orbitals (94%) with a very small contribution from Zn (6%) (Figure S20). In contrast, the lowest unoccupied molecular orbital (LUMO) has a significant character of Zn orbitals (54%), along with some residual Ge-Ge bonding character (46%). The large HOMO–LUMO gap of 2.22 eV found in both $[Zn_6Ge_{16}]^{4-}$ and $[Cd_6Ge_{16}]^{4-}$, preclude any second-order Jahn–Teller instabilities, consistent with the rigorous T_d symmetry. It should be noted that the absolute values of the HOMO–LUMO gaps depend on the amount the Hartree–Fock exchange, and, hence, should be treated with caution. Typically, large HOMO–LUMO gaps suggest high kinetic stability and usually relate to aromatic compounds, which also exhibit high-symmetry structures.[13] To better understand the reasons of the stability of these clusters, a more thorough chemical bonding analysis was developed. Because of the complexity of the canonical molecular orbitals (CMOs), which are intrinsically difficult to interpret in terms of chemical bonds due to delocalization, Adaptive Natural Density Partitioning (AdNDP)[14] analysis was performed as implemented in AdNDP 2.0 code.[15] The AdNDP algorithm has previously been used with great success to analyze chemical bonding patterns in a wide range of inorganic Zintl anions.[16] The $[M_6Ge_{16}]^{4-}$ clusters have 140 valence electrons in total (12 | e | from each M-atom, 4 | e | from each Ge-atom and 4 | e | from the 4− overall charge), giving rise to 70 two-electron AdNDP bonding elements. According to AdNDP, there are five *d*-type lone

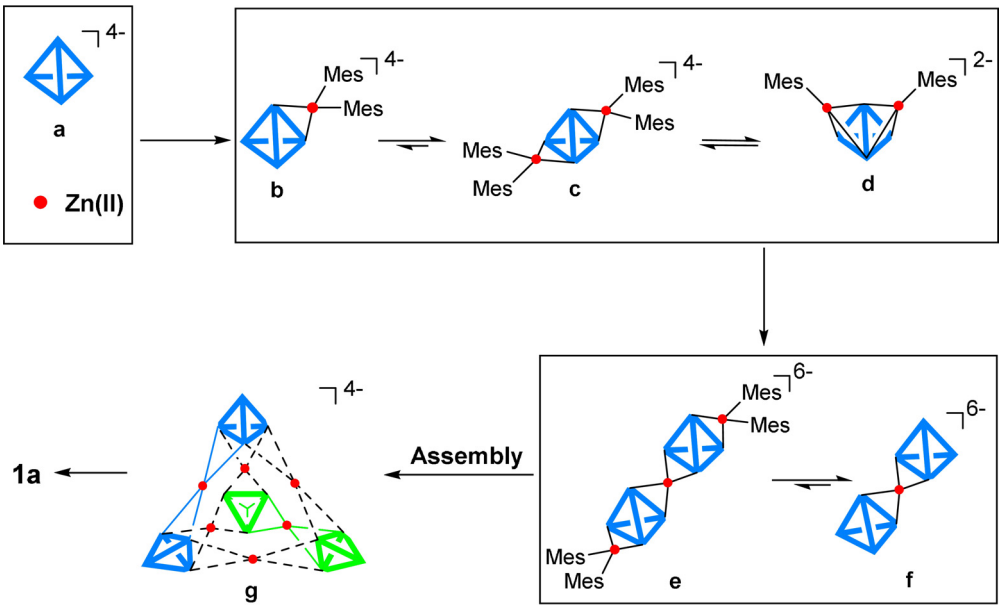

Figure 2. The assembly mechanism of tetrahedral cluster $[Zn_6Ge_{16}]^{4-}$. Species that have been observed in the mass spectra are boxed (**c**, **d**, **e**, **f**, **1a**).

pairs on each M atom, and one s-type lone pair on each Ge atom, thus accounting for 46 electron pairs (Figure S21, S22). The remaining 24 pairs (48 electrons) form twelve 3c-2e Ge-Ge-Ge σ bonds (three per Ge_4) (Figure 3A) and twelve 3c-2e M-Ge-Ge σ bonds (three per Ge_4) (Figure 3B). Alternatively, twelve 3c-2e Ge-Ge-Ge σ bonds could also be viewed as twelve more localized 2c-2e Ge-Ge σ bonds located over the Ge_4 edges with lower occupation numbers (Figure S23). To complement the AdNDP localization, we have also explored

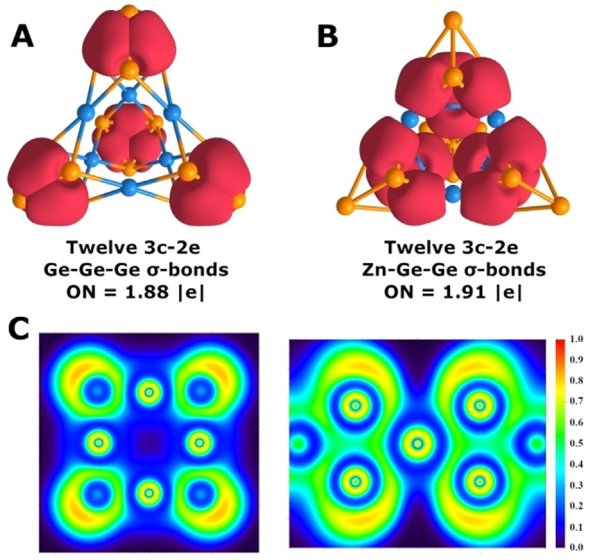

Figure 3. A) 3c-2e Ge-Ge-Ge σ-bonds of $[Zn_6Ge_{16}]^{4-}$ shown superimposed on the molecular framework (three bonds per Ge_4); B) 3c-2e Zn-Ge-Ge σ-bonds of $[Zn_6Ge_{16}]^{4-}$ shown superimposed on the molecular framework (three bonds per Ge_4); C) ELF distribution in rectangular Ge_4Zn fragment (right) and square Zn_4 fragment (left). ON denotes occupation number. Exactly the same AdNDP and ELF pictures are identified for $[Cd_6Ge_{16}]^{4-}$, both are omitted for clarity.

the topology of the Electron Localization Function (ELF), η(r),[17] 2D plots of which are plotted for selected planes in Figure 3C. In agreement with the 3c-2e M-Ge-Ge σ bonds, there is a clear localization in the M-Ge-Ge region (in the plane of Ge_4M fragment, Figure 3C(left)), with the major contribution coming from the two Ge atoms. In contrast, the ELF is close to zero in the cavity at the center of the cluster (Figure 3C(right)), supporting the absence of the M-M interactions in the M_6 octahedron.

The major contribution to the 3c-2e M-Ge-Ge σ bonds comes from two Ge atoms (84% in $[Zn_6Ge_{16}]^{4-}$ and 86% in $[Cd_6Ge_{16}]^{4-}$). However, the substantial delocalization over the M center drives the elongation of the coordinated Ge-Ge bonds, which are significantly longer than the sum of the Ge covalent radii for a single Ge-Ge bond, that is, 2.42 Å.[18] In fact, the M contribution in each 3c-2e σ bond is significant, that is, 0.30 | e | . Hence, the stability of the $[M_6Ge_{16}]^{4-}$ clusters may not be ascribed to pure ionic interactions of M^{2+} cations stabilizing the $[Ge_4]^{4-}$ anionic tetrahedra. The appreciable covalent character arises due to the delocalization over the M atom which is, in total, 0.60 | e | per two 3c-2e bonds formed by one M atom. In this sense, the oxidation state of the transition metal ions is intermediate between 1+ and 2+. It is worth noting that the Au^{1+} and Ag^{1+} compounds have previously been shown to adopt similar planar tetracoordinate configurations of these coinage metals with tetrahedral sub-units composed out of Sn, Sb, or As atoms.[4,19] As evident from the natural electron configuration of Zn in $[Zn_6Ge_{16}]^{4-}$ ($4s^{0.84}4p^{0.88}3d^{9.98}$), there is a considerable covalency that leads to a build-up of the electron density in Zn 4s and 4p, leading to the sp-hybridization.

Based on the most employed criterion of aromaticity, that is, the magnetic criterion that assumes that an aromatic fragment sustains ring current because of its delocalized electrons, we further calculated magnetic response properties of the $[M_6Ge_{16}]^{4-}$ clusters (E = Zn or Cd), which involves four spherical aromatic $[Ge_4]^{4-}$ fragments, as shown earlier by Hirsch and co-workers (a detailed discussion on why $[Ge_4]^{4-}$ is regarded as spherically aromatic can be found in the Supporting Information).[20] In order to obtain a global view of the aromatic character, we computed the induced magnetic field (B^{ind}_{iso}) in terms of isotropic ($B^{ind}_{iso} = -(1/3)(\sigma_{xx}+\sigma_{yy}+\sigma_{zz})B^{ext}$) (orientational average) and for particular orientations of the external field (Figure 4, see the Supporting Information for computational details). In general, for

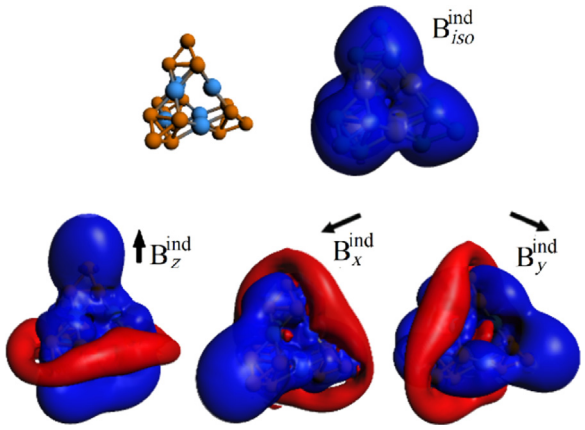

Figure 4. Magnetic response properties of $[Zn_6Ge_{16}]^{4-}$, given by isotropic term (B^{ind}_{iso}), and under specific orientations of the external field (B^{ind}_{z}, B^{ind}_{x}, and B^{ind}_{y}). Isosurfaces at ±5 ppm; Blue: shielding; Red: deshielding. The same features are found for $[Cd_6Ge_{16}]^{4-}$ (Figure S24).

spherical aromatic clusters, such as $[Ge_4]^{4-}$, B^{ind}_{iso} exhibits a spherical-like shielding region. For $[M_6Ge_{16}]^{4-}$ clusters, B^{ind}_{iso} shows four spherical-like shielding regions connected via Zn^{2+} or Cd^{2+}, denoting four spherical aromatic Ge_4 fragments, indicating that in the self-assembly of $[Ge_4]^{4-}$ building blocks in the ionic limit, their aromatic character is retained. This suggests that a convenient strategy for designing controlled aggregates can be based on aromatic building blocks prone to be connected by d^{10} ions nodes. Indeed, under specific orientations of the field, the characteristic shielding cone is enabled with a complementary perpendicular deshielding, resembling the characteristics of planar Hückel aromatics. In the case of $[M_6Ge_{16}]^{4-}$ clusters, the different long-range shielding regions are overlapped resulting in a global induced magnetic field, unraveled as a characteristic of the tetrahedral cluster aggregates. Overall, these results reveal the aromatic character of 3c-2e Ge-Ge-Ge σ bonds, where 3c-2e M-Ge-Ge σ bonds are also involved in the spherical aromatic character of connected $[Ge_4]^{4-}$ blocks. Thus, the global aromatic character of $[M_6Ge_{16}]^{4-}$ species is determined by the addition of the individual spherical aromatic behavior of each Ge_4 fragment. The aromatic ring currents from the Ge_4 fragments generate the obtained shielding regions, which are superimposed. Hence, a superimposed ring current is expected to occur in the $[M_6Ge_{16}]^{4-}$ clusters in the magnetic field.

In summary, the supertetrahedral frameworks in the anionic components of **1a** and **2a**, are formed from the assembly of smaller $Zn_x(Ge_4)_y$ fragments, driven by the strong Zn-Ge-Ge interactions via three delocalized 3c-2e σ bonds per Ge_4. Self-assembly processes of this type may open the door to new ligand-free metal-framework-based materials. Therefore, it represents a potential strategy for constructing many new heterometallic nanoclusters using other lower charged transition metal cations and tetrahedral cluster precursors as subunits, such as $[E_2Pn_2]^{2-}$ or $[E_3Pn]^{3-}$ (E = Ge, Sn, Pb; Pn = P, As, Sb, Bi), where spherical aromatic clusters are suggested as stable building blocks. Detailed AdNDP and ELF analyses confirmed that the stability of the $[M_6Ge_{16}]^{4-}$ clusters may not be ascribed to pure ionic interactions of M^{2+} cations stabilizing the $[Ge_4]^{4-}$ anionic tetrahedra. The appreciable covalent character arises due to the delocalization over the M atom by forming 3c-2e M-Ge-Ge σ bonds. Due to the substantial contribution of M atoms in these delocalized bonds, the oxidation state of the M atoms may be considered as intermediate between 1 + and 2 + . The calculations of the magnetic response properties reveal the aromatic character of 3c-2e Ge-Ge-Ge σ bonds, where 3c-2e M-Ge-Ge σ bonds are also involved in the spherical aromatic character of connected tetrahedral blocks, thus explaining the stability of the $[M_6Ge_{16}]^{4-}$ clusters. Based on the chemical bonding analyses of $[M_6Ge_{16}]^{4-}$, it is expected to see that similar supertetrahedral clusters with planar tetracoordinate monovalent metal ions (e.g. Au^{1+}, Ag^{1+}) coordinating to the tetrahedral {Ge, Sn, Sn, Sb, or As}-based fragments may also be viable.

Acknowledgements

This work was supported by the National Natural Science Foundation of China (21971118 and 21722106 to Z.M.S.) and the USA National Science Foundation (grant CHEM-1664379) to A.I.B. This work was supported by the US Department of Energy through the Los Alamos National Laboratory. Los Alamos National Laboratory is operated by Triad National Security, LLC, for the National Nuclear Security Administration of the U.S. Department of Energy (Contract No. 89233218CNA000001). I.A.P. acknowledges support from J. Robert Oppenheimer Distinguished Postdoctoral Fellowship at the Los Alamos National Laboratory. The support and resources from the Centre for High Performance Computing at the University of Utah are gratefully acknowledged.

Conflict of interest

The authors declare no conflict of interest.

Keywords: planar tetracoordinate Zn/Cd · supertetrahedron · T_d symmetry · Zintl clusters · σ-aromaticity

[1] a) N. F. Zheng, X. H. Bu, P. Y. Feng, *Nature* **2003**, *426*, 428 – 432; b) M. Duchardt, U. Ruschewitz, S. Adams, S. Dehnen, B. Roling, *Angew. Chem. Int. Ed.* **2018**, *57*, 1351 – 1355; *Angew. Chem.* **2018**, *130*, 1365 – 1369.

[2] a) J. Li, X. Li, H.-J. Zhai, L.-S. Wang, *Science* **2003**, *299*, 864 – 867; b) E. S. Kryachko, F. Remacle, *Int. J. Quantum Chem.* **2007**, *107*, 2922 – 2934; c) D.-E. Jiang, M. Walter, *Phys. Rev. B Condens. Matter* **2011**, *84*, 193402.

[3] a) Z. Wu, Y. Du, J. Liu, Q. Yao, T. Chen, Y. Cao, H. Zhang, J. Xie, *Angew. Chem. Int. Ed.* **2019**, *58*, 8139 – 8144; *Angew. Chem.* **2019**, *131*, 8223 – 8228; b) S. Kenzler, F. Fetzer, C. Schrenk, N. Pollard, A. R. Frojd, A. Z. Clayborne, A. Schnepf, *Angew. Chem. Int. Ed.* **2019**, *58*, 5902 – 5905; *Angew. Chem.* **2019**, *131*, 5962 – 5966.

[4] F. X. Pan, L. J. Li, Z. M. Sun, *Chin. J. Struct. Chem.* **2016**, *35*, 1099 – 1106.

[5] a) C. B. Benda, M. Waibel, T. Kochner, T. F. Fässler, *Chem. Eur. J.* **2014**, *20*, 16738 – 16746; b) R. J. Wilson, N. Lichtenberger, B. Weinert, S. Dehnen, *Chem. Rev.* **2019**, *119*, 8506 – 8554; c) "Binary and Ternary Intermetalloid Clusters. Clusters—Contemporary Insight in Structure and Bonding": B. Weinert, S. Dehnen in *Structure and Bonding*, *Vol. 174* (Eds.: S. Dehnen), Springer, Cham, **2017**, pp. 99 – 134; d) C. Wallach, K. Mayer, T. Henneberger, W. Klein, T. F. Fässler, *Dalton Trans.* **2020**, *49*, 6191 – 6198.

[6] a) H. G. von Schnering, J. Llanos, J.-H. Chang, K. Peters, E.-M. Peters, R. Nesper, *Z. Kristallogr. New Cryst. Struct.* **2005**, *220*, 324; b) T. Henneberger, W. Klein, J. V. Dums, T. F. Fässler, *Chem. Commun.* **2018**, *54*, 12381 – 12384.

[7] a) K. Mayer, L. J. Schiegerl, T. F. Fässler, *Chem. Eur. J.* **2016**, *22*, 18794 – 18800; b) K. Mayer, L. A. Jantke, S. Schulz, T. F. Fässler, *Angew. Chem. Int. Ed.* **2017**, *56*, 2350 – 2355; *Angew. Chem.* **2017**, *129*, 2390 – 2395; c) J. M. Goicoechea, S. C. Sevov, *Organometallics* **2006**, *25*, 4530 – 4536; d) F. Henke, C. Schenk, A. Schnepf, *Dalton Trans.* **2009**, 9141 – 9145; e) S. Stegmaier, T. F. Fässler, *Inorg. Chem.* **2013**, *52*, 2809 – 2816; f) M. Waibel, T. Henneberger, L. A. Jantke, T. F. Fässler, *Chem. Commun.* **2012**, *48*, 8676 – 8678; g) C. B. Benda, R. Schäper, S. Schulz, T. F. Fässler, *Eur. J. Inorg. Chem.* **2013**, 5964 – 5968.

[8] a) S. Stegmaier, M. Waibel, A. Henze, L.-A. Jantke, A. J. Karttunen, T. F. Fässler, *J. Am. Chem. Soc.* **2012**, *134*, 14450 – 14460; b) V. Queneau, S. C. Sevov, *J. Am. Chem. Soc.* **1997**, *119*, 8109 – 8110.

[9] S. Mitzinger, J. Bandemehr, K. Reiter, J. S. McIndoe, X. Xie, F. Weigend, J. F. Corrigan, S. Dehnen, *Chem. Commun.* **2018**, *54*, 1421 – 1424.

[10] C. Adamo, V. Barone, *J. Chem. Phys.* **1999**, *110*, 6158 – 6169.

[11] F. Weigend, R. Ahlrichs, *Phys. Chem. Chem. Phys.* **2005**, *7*, 3297 – 3305.

[12] Gaussian 16, Revision B.01, M. J. Frisch, G. W. Trucks, H. B. Schlegel, et al., Gaussian, Inc., Wallingford CT, **2016**.

[13] J. M. Mercero, A. I. Boldyrev, G. Merino, J. M. Ugalde, *Chem. Soc. Rev.* **2015**, *44*, 6519 – 6534.

[14] D. Y. Zubarev, A. I. Boldyrev, *Phys. Chem. Chem. Phys.* **2008**, *10*, 5207 – 5217.

[15] N. V. Tkachenko, A. I. Boldyrev, *Phys. Chem. Chem. Phys.* **2019**, *21*, 9590 – 9596.

[16] a) I. A. Popov, F.-X. Pan, X.-R. You, L.-J. Li, E. Matito, C. Liu, H.-J. Zhai, Z.-M. Sun, A. I. Boldyrev, *Angew. Chem. Int. Ed.* **2016**, *55*, 15344 – 15346; *Angew. Chem.* **2016**, *128*, 15570 – 15572; b) I. A. Popov, A. A. Starikova, D. V. Steglenko, A. I. Boldyrev, *Chem. Eur. J.* **2018**, *24*, 292 – 305; c) N. V. Tkachenko, A. I. Boldyrev, *Chem. Sci.* **2019**, *10*, 5761 – 5765; d) C. Liu, N. V. Tkachenko, I. A. Popov, N. Fedik, X. Min, C.-Q. Xu, J. Li, J. E. McGrady, A. I. Boldyrev, Z.-M. Sun, *Angew. Chem. Int. Ed.* **2019**, *58*, 8367 – 8371; *Angew. Chem.* **2019**, *131*, 8455 – 8459.

[17] a) B. Silvi, A. Savin, *Nature* **1994**, *371*, 683 – 686; b) T. Lu, F. Chen, *J. Comput. Chem.* **2012**, *33*, 580 – 592.

[18] P. Pyykkö, *J. Phys. Chem. A* **2015**, *119*, 2326 – 2337.

[19] C. Schwarzmaier, M. Sierka, M. Scheer, *Angew. Chem. Int. Ed.* **2013**, *52*, 858 – 861; *Angew. Chem.* **2013**, *125*, 891 – 894.

[20] A. Hirsch, Z. Chen, H. Jiao, *Angew. Chem. Int. Ed.* **2001**, *40*, 2834 – 2837; *Angew. Chem.* **2001**, *113*, 2916 – 2920.

Manuscript received: June 10, 2020
Accepted manuscript online: June 30, 2020
Version of record online: August 13, 2020

